Characterization of EMAT Guided Wave Reflectivity on Welded Structures for use in Ranging

Ross McMillan, Morteza Tabatabaeipour, Rory Hampson, Charalampos Loukas, Taiyi Zhao, Rachel S. Edwards, Charles Macleod and Gordon Dobie

***Abstract*— Guided wave ranging measurements offers an elegant method to localize an inspection robot relative to the geometric features, such as welds, of a structure under test. This paper characterizes the suitability of various EMAT generated guided wave modes when reflecting from butt welds for the purpose of choosing a low frequency mode suitable for accurate ranging. Wave modes were tested in 10mm mild steel plate in experiment and simulation, the method of data extraction is discussed as well as the determination of the wave mode best suited for weld ranging by means of comparison of the reflection coefficients. The authors conclude SH1 at a frequency-thickness product of 2 MHz.mm, is shown to be a highly suitable wave mode for gaining a large reflection from a weld, with an average reflection co-efficient of approximately 0.45 across four different sized weld crowns. A ranging over 1 meter experimentally was demonstrated to have a 2.65% error using our method. This work will enable simultaneous detailed mapping through ranging and inspection of large welded structures by mobile robotic inspection systems using EMAT's.**

***Index Terms*— Automation/Robotics, EMATs. Guided Waves, Guided Wave Reflectivity, Weld Detection.**

I. Introduction

STRUCTURAL assets such as large tanks/vessels and structural components naturally decay through corrosion and cracking. Robotic non-destructive inspection/testing (NDI/NDT) can be used to assess the integrity of these assets so they can be maintained appropriately and safely [1]–[4]. Robotic inspection can either be performed by an operator or automatically, but each carries the same burden of needing to know where the robot is during the inspection, this is an ongoing challenge in mobile robotics called robot localisation [5].

Authors on this work have previously shown that using structure-borne ultrasonic guided waves has promise for robust robot localisation and mapping [6]. In order for a mobile robot to localise on features within a subject, guided waves must be able to consistently reflect from features and then subsequently the reflections should be able to be used to accurately determine the position of the feature relative to the sensors, this is ranging using reflected guided waves [7].

The structures that are intended to be inspected by the system in [6] are large tankers and vessels similar to that shown in the Abstract Figure, which are considered plate-like structures joined with welds. Welds are an extremely common feature on these structures so are ideal for use as a consistent reflector for a mobile robot to range from. Although these are cylindrical, pipe like structures, due to the shallow curvature they can be considered plate-like, [8] shows that if the radius:thickness ratio is greater than 10:1 the effect of plate curvature on the dispersion curves is negligible.

There are two main ultrasonic guided wave modes that can be generated in plate-like structures, Lamb waves and Shear Horizontal waves [9]. Non-contact guided waves are commonly generated using Electromagnetic Transducers (EMATS) which typically use a pulsed coil and static magnetic field to generate a guided wave [9]–[12]. EMATs are suited to mobile robotics where contact with the subject is not required to generate a wave which in turn will not impede the movement of the crawler. Rayleigh waves are surface waves, similar to guided waves, which can also be generated using EMATs [13].

A. Guided Waves and Welds

Ultrasonic weld inspection can be undertaken using multiple methods, from traditional ultrasonic inspection [14]–[17], to phased array measurement [18]–[20], guided wave inspection [21]–[26], and evaluation using weld-guided waves [27]–[29].

For the majority of research on the topic of weld inspection using ultrasonic methods, the detection of defects within the weld has been investigated rather than the reflections from the weld. The focus of this work is to achieve local ranging by reflecting transmitted guided waves off of welds in order to localise the robot, so in this case the weld is instead a useful tool and is not impeding inspection.

Little work has been conducted on the reflectivity of guided wave modes from welded features and sections. Existing work [30] has looked at the propagation of SH0, 128kHz, waves at a Butt Weld, T-Joint, and Lap Joint. SH0 was shown to reflect off each weld type in experimental setup and 2D simulation, however the reflections were found through non-welded area comparisons.

Khalili and Cawley [31] used simulation to carry out an investigation into the response of SH0, SH1, S0 and A1 modes when encountering features in 10mm steel. It was found that S0, SH0 and SH1 were reflected from a T-joint, with SH1 having the highest reflection coefficient. The T-Joint was simulated by adding additional steel to the surface of the plate without simulating any weld head or weld pass geometry. 2DFFT was used to identify the modes.

Sargent [32] used an omnidirectional multi-element transducer to detect corrosion within butt welds and did not measure wave mode reflectivity. It is stated that at positions normal to the weld the reflectivity of the S1 wave mode was too great to identify the artificial corrosion.

Both [33] and [34], investigated Rayleigh wave interaction with welds and rib type features (geometry comparable to butt welds), showing instances of Rayleigh wave reflections at very short distances with low reflectivity.

The literature presented does not provide a thorough and complete investigation into guided wave reflectivity from butt welds, this information is needed for the proposed application. As a result ranging using guided waves from welds has not been investigated, which must be done to allow for the positioning of robots deploying EMATs on welded structures.

B. This Work

To assess whether a guided wave mode is capable for use in ranging using welds, its reflectivity from welds must first be investigated, as if the mode cannot reflect well from welds it is not suitable for ranging. The following wave modes were investigated: SH0 (128 kHz), SH1 (205 kHz), S0 (106 kHz), S1 (375 kHz) and A0 (91 kHz). The modes listed are marked on a dispersion curve for 10mm Mild Steel, Fig. 1. SH0 was previously used in [6] but only for reflection from edges, so had to be evaluated for use on welds. SH frequencies were chosen based on the EMAT's available for experimental generation and Lamb wave frequencies were chosen where dispersion would be reduced and encouraged single mode generation.

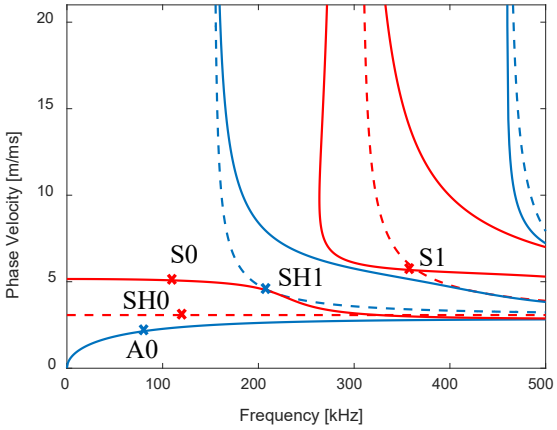

Fig. 1 Theoretical dispersion curve for guided waves in 10mm thick steel. Lamb (solid lines) and Shear Horizonal (dashed lines) wave modes are shown. Asymmetric modes are blue and symmetric modes are red, this graph was generated using the Dispersion Calculator Software (Centre for Lightweight Production Technology, DE). X's represent the frequencies of the wave modes used in this work.

A1 was not selected as in [31] it was found to have no reflection on the T-Joint weld. Rayleigh waves have previously been shown to have a small reflection coefficient from welds [33], [34]. However, their propagation distance is typically shorter than guided wave modes such as Lamb or SH waves. In addition, the wavelengths required to ensure that the wave in a 10mm thick plate behaves as a Rayleigh-like wave are very small, and hence will be strongly attenuated by very small surface defects [36].

The wave mode best suited to ranging from welds requires the characteristics described in the following paragraphs. Strong reflectivity from welds is the most important factor to consider when selecting the wave mode best suited for the localisation system, if the mode does not reflect off of welds then ranging is not possible. Greater reflectivity makes it easier to do Time-of-Fight (TOF) calculations for ranging. A greater reflectivity shows that welds are easily detectable by the mode and can be distinguished from other features.

A particular weld is likely to have variations in its geometry across its length, so it is preferred that wave mode reflectivity is consistent with weld size and would increase linearly and proportionally to a weld heads geometry that increases in size, as well when the weld decreases in size, the reflectivity reduces proportionally.

Low dispersion is desirable when dealing with guided waves. The range of wave propagation this system will be operating within is up to 2m, at this shorter range dispersion was found to be manageable. Fig. 2 shows SH1 signals for receiver positions at 200mm and 600mm from the weld, the weld reflection is identifiable even when the wave has a total travel path, from transmission point to the weld and reflecting back to receiver, of 1.5m.

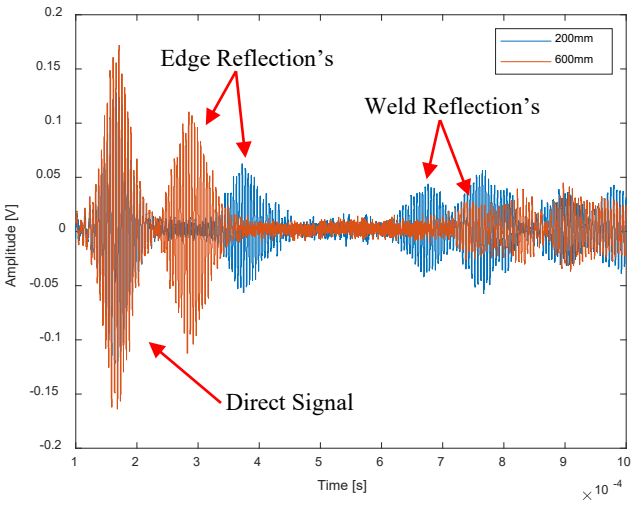

Fig. 2 Experimental data. First received direct signal, left edge reflection signals and weld signals are highlighted. SH1 at 205kHz was used on Sample 3 for these measurements. The blue signal is where the receiver is 20cm from the weld and the orange signal is where the receiver is 60cm from the weld.

To investigate the chosen modes Finite Element Analysis was used to sweep through the range of variables that could not be evaluated experimentally. Simulations were validated experimentally on a subset of wave modes.

This paper is arranged as follows. Section II covers the background theory on what wave mode characteristics result in a high reflection coefficient, Section III covers the simulation setup and results of the simulations ran. Section IV covers the experimental setup, results and comparison of simulation and

experimental results. Section V covers ranging testing usability for real world practicality.

II. Methodology

The wave modes indicated in Fig. 1 were investigated in 10mm S275-N Steel plate as this is commonly used in the construction of large oil and gas industry plant [37]. The material used is mild steel and as shown in [38] and [39] the grain structure of a parent metal and bead added via MIG welding is approximately the same size, 34µm. The HAZ will have significantly less effect on the reflection of the wave than the geometry changes of the bead, especially in the case of the samples used in this work, as such grain structure is not explored in simulation.

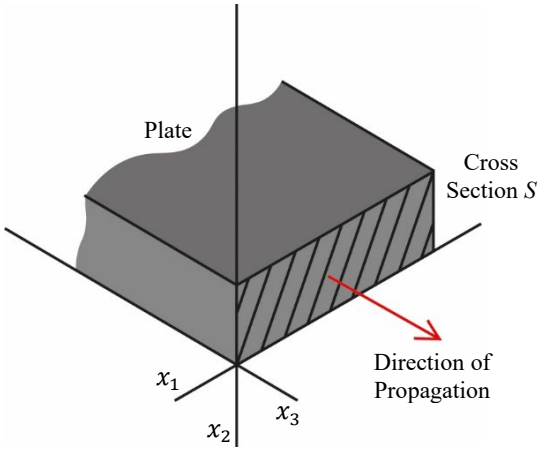

Fig. 3 The coordinate system shown here is depicted with a plate to better illustrate the direction of wave propagation and the cross section, S, which is in the $x_1 - x_2$ plane.

Considering the geometry of a weld on plate, the presence of a weld head causes an increase from nominal plate thickness, the wave mode which is best suited to ranging will react to this change in thickness by strongly reflecting from it. This requires the mode to be sensitive to upper and lower boundary changes. The energy density distribution of a wave mode, for a given plate thickness, can be used to identify the areas of a plate thickness which carry the largest portions of a waves energy, as this is not always constant across the thickness. The energy density distribution, E_{total}, can be calculated for a given point in the plates thickness using Equations 1-3. These equations operate in a domain, $x_i = (x_1, x_2, x_3)$, see Fig. 3, where the plate thickness is on the x_2 axis, this is the axis the values in Fig. 4 are calculated for.

$$E_{total} = E_{strain} + E_{kinetic} \quad (1)$$

$$E_{strain} = \frac{1}{2}\int_s \sigma_{ij}\,\varepsilon_{ij} dS \qquad i,j = 1,2,3, \quad (2)$$

$$E_{kinetic} = \frac{1}{2}\rho \int_s v_i^2\, dS \quad (3)$$

Where σ_{ij} is the stress tensor, ε_{ij} is the strain tensor, ρ is the plate density, v_i is the particle velocity, integration of the two energy densities is performed over the cross section of the plate, S [40].

Analysis of the energy density distributions of the chosen wave modes across plate thickness, shows that A0, S1 and SH1 have a higher percentage of the wave energy at the plate boundaries rather than the centre of the plate thickness, as shown in Fig. 4. The upper and lower boundaries of the plate are where the thickness increases when a weld head is present, and it is thought that modes which have an energy distribution favouring the plate boundaries will reflect well from welds.

Reflectivity is also thought to be dependent on low mode conversion at geometric changes in a subject where thickness variation occurs. Most geometric features can be described as a thickness change [41]. A significant amount of work has been conducted into mode conversion of guided waves when encountering thickness changes within a subject [9], [41]–[45].

It is hypothesised that the ideal mode for useful high reflectivity will have an energy distribution favouring boundaries and has low mode conversion when encountering plate thickness changes, such as SH1 or S1, which shall be validated in this work.

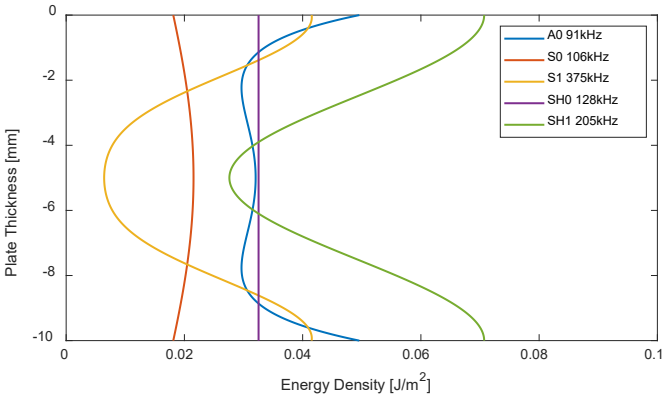

Fig. 4 Energy density (E_{total}) distributions across 10mm plate for A0, S0, S1, SH0 and SH1 generated using Dispersion Calculator.

III. Simulation

A. Measurement Setup

The setup described below was used for both simulation and experiment. To obtain reflection coefficient values, the wave modes were propagated at a weld head. A transmitter generates the wave which is directed towards the receiver to measure an initial signal, this setup is shown in Fig. 5. Depending on the mode it will not reflect, reflect or strongly reflect off of the weld and propagate back to the receiver. Using a 2DFFT based method the amplitude of the weld reflection signal and the first received signal can be obtained to gain a reflection coefficient value. As the setup will remain the same for each wave mode investigated, the values for each wave mode can be easily compared.

Transmitter and receiver EMAT's are separated 300mm colinearly centre to centre. Experimentally the receiver is moved in 1mm steps over 64mm to allow a 2DFFT to be performed on the data. In simulation the steps are modelled as nodes, spaced similarly, which measure directional velocity changes over time. The transmitter/receiver setup is placed so that the receiver is 400mm from the weld. Plate dimensions are 1.5x0.3x0.01m where the weld is 500mm from the right-hand edge, this setup is the same for the experimental plates.

Each of the modes were propagated at four weld heads with different geometries. Different weld heads were used to characterise a given wave modes reaction to small changes in weld geometry.

The calculated weld head Cross Sectional Area (CSA) for each weld head is given in Table 2, It is thought that the larger the CSA the higher the reflectivity. The different weld heads were manufactured, measured, and then modelled using Solidworks (Dassault Systems, FR), in simulation the weld microstructure [32], [46] was not modelled. It is thought to have some effect on the reflectivity of a wave mode but not significant [47], [48].

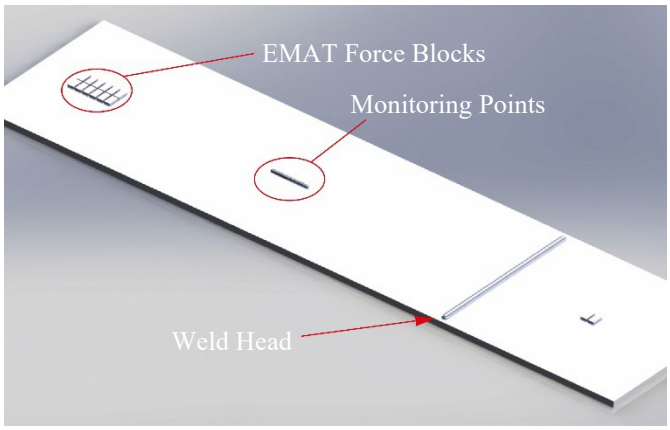

Fig. 5 The weld sample model with the PPM EMAT block representations and monitoring point representations for SH wave inspection, which allow measurement at 64 different points with 1mm spacing.

The EMAT model used to generate SH modes was a 6x2 magnet PPM (Periodic Permanent Magnet) configuration, where magnet dimensions were 20x10x5mm [22]. The EMAT's were modelled from Sonemat (Sonemat Ltd., UK) sensors that were used for experimental measurement. OnScale (OnScale, US-CA) was used to run the simulations. The PPM EMAT model was used to generate SH0 (128kHz, 25mm wavelength) and SH1 (205kHz, 25mm wavelength) in simulation.

To generate S0 (106kHz, 51mm wavelength), S1 (375kHz, 16.1mm wavelength), and A0 (91kHz, 25.4mm wavelength) modes, a meander coil EMAT was simulated [49]–[51].

A 5-cycle sinusoidal pulse was used as the driving function [6]. 0.5mm mesh size was used for this model as a compromise between numerical stability and computational time vs. the time step for the Courant–Friedrichs–Lewy (CFL) stability criterion [52] . Plate density was set to 7850kg/m^3 [53].

B. Data Extraction

To calculate the reflection coefficient values for the waves propagated in simulation and experimentally, a 2DFFT [20] was performed on the data to gain an accurate value of the amplitude of the initial signal and the reflected signal. 2DFFT is suitable for use with dispersive and non-dispersive modes [31]. This can be used to better extract information from multiple A-Scans by taking measurements in the spatial domain as well as the time domain allowing isolation of specific frequencies and their amplitudes [54]–[56]. 2DFFT is also used to validate the wave modes generated experimentally and in simulation [55], [57].

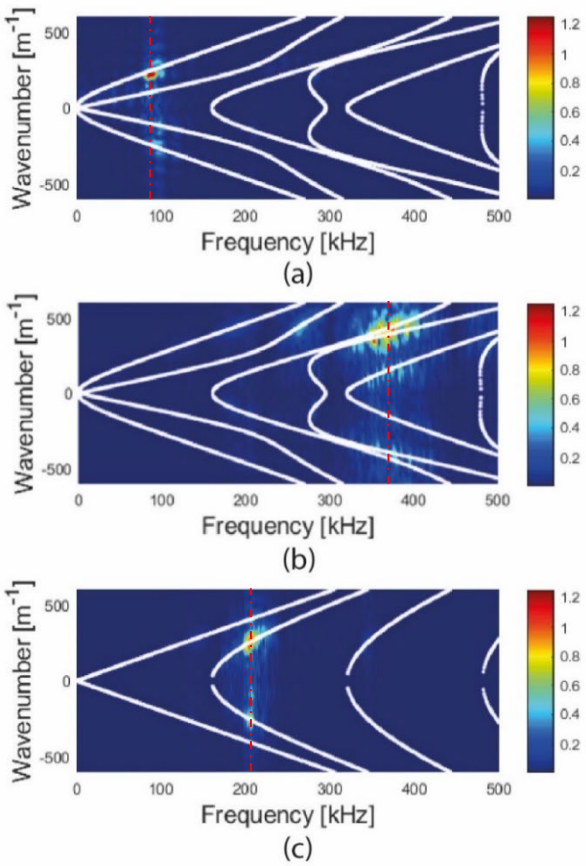

Fig. 6 Wavenumber-Frequency Amplitude plots for (a) A0 (91kHz) (b) S1 (375kHz) (c) SH1 (128kHz). The centre frequencies are highlighted. The mode conversion of the generated waves and the waves that returned after reflecting from the weld, are those with negative wavenumbers.

To find the reflection coefficient for a given wave mode and weld size the following steps were taken:

1) 64 measurements were taken at intervals of 1mm, monitoring points in Fig. 5, where the receiver moves and the transmitter remains stationary to form a 2D array data set. A specific time period is isolated so that only the first transmitted wave and the weld reflected wave are considered.

2) A 2DFFT is performed on this data which builds a 2D plot, Fig. 6, where it is organised by wavenumber, frequency and amplitude. A theoretical dispersion curve plot is overlaid as well. As mode conversion can occur at the weld reflection, and dispersion causes parts of the wave to spread out; using 2DFFT counteracts this by organising amplitude by frequency and wavenumber, instead of by time.

3) A vertical line at the centre frequency for the generated mode is drawn, to isolate this frequency, and the point where this line intersects the dispersion curve is isolated within this plot and a wavenumber amplitude graph is generated for positive and negative wavenumbers, see Fig. 7 [58].

4) Using the wavenumber amplitude plot, the spikes which represent the first transmitted and first weld reflected waves can be identified. Integration is then performed on each spike to calculate the area under the spike, this is more accurate than taking the max amplitude value as it considers the changes in the width of the signal.

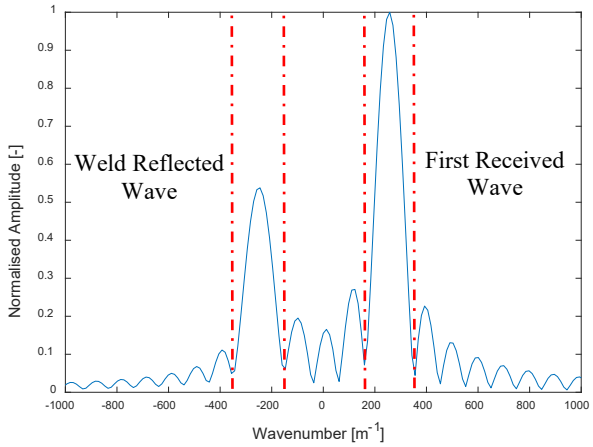

Fig. 7 An example of the Normalised Amplitude-Wavenumber plot that is used to find the magnitude of the first transmitted wave and the weld reflected wave, this example is for SH1 taken from the plot Fig 6c. The limits of the integration performed on the spikes are highlighted by the red dashed lines.

5) To find the reflection coefficient the area of the weld reflection spike is then divided by the area of the received signal spike, Fig. 7. Using this method the individual wave modes can be isolated, and the reflectivity calculated.

Using material datasheets [53], wave properties were calculated for the S-275N samples, including theoretical longitudinal and shear velocities [59]. To verify these values, bulk ultrasonic wave measurements and Time of Flight calculations were carried out on the experimental samples. The results for both theoretical and experimental values are shown in Table 1.

Table 1- Sample Longitudinal and Shear Velocities

	Longitudinal Velocity (m/s)	Shear Velocity (m/s)
Material Calculated Values	6001	3208
Experimental Test Values	5959	3259

C. Wave Mode Focused Simulation Results

Results for the wave mode focused simulations are graphed in Fig. 8. When analysing the data to calculate the reflection coefficient for the simulated modes, S1 showed significant mode conversion. A0, S1 and SH1 were focussed on during analysis due to the characteristics of their plate thickness energy distributions. Fig. 6, shows the wavenumber-frequency distributions of A0, S1 and SH1, for direct and reflected signals, these modes have similar energy distributions which favour the boundaries of the plate. Significant amounts of mode conversion occur for S1 upon generation and when interacting with the weld, this made analysis difficult due to the noisy returning signal, this was also found in [32].

For the frequency of A0 tested, minimal amounts of mode conversion to S0 occurs upon generation. A small amount of energy is reflected in equal amounts from A0 and S0, this indicates that mode conversion is occurring when the wave encounters the weld.

In simulation SH1 was found to be the most reflective out of the modes propagated, as in Table 5 of [31] where SH1 was found to have the highest reflection coefficient however the focus of this paper was corrosion detection not ranging. SH1 showed the most desirable response for ranging by having the highest reflection coefficient and the reflectivity value changes were proportional to weld geometry changes.

Comparing the energy density distributions, Fig. 4, to Fig. 6, where the level of mode conversion for A0, S1 and SH1 can be seen. SH1 has the thickness energy distribution which best favours the boundaries of the plate, almost no mode conversion and it has the highest reflection coefficients found. This shows that the findings in simulation align with the theory discussed in Section II. Although S1 has the second highest reflectivity, this was not able to be validated experimentally due to project limitations, as such SH0 was tested instead. Fig. 4 shows that SH0 has a higher average energy density than S1 so is a suitable replacement in experiment.

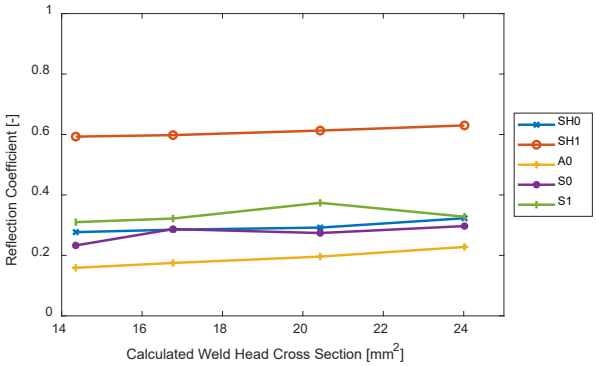

Fig. 8 Simulated data. The reflection coefficient for each mode and each sample is shown, SH1 is significantly more reflective than the other modes tested, S1 is the most reflective lamb mode. Good stability is shown by A0, SH0 and SH1.

IV. Experiment

A. Weld Samples

Four 10mm S275-N Steel plates were used as the parent material of base test geometries. To minimise the variables within the experimental setup and to ease the manufacture process, weld beads were added straight to parent plates via Metal Inert Gas (MIG) welding, instead of directly butt welding two plates together. This enabled the geometry of the plate and weld cap to be representative but with minimal plate distortion on each side of the weld bead.

Table 2 lists the weld head geometry of the four samples, the weld on each plate was positioned 0.5m from the right-hand edge. The geometry measurements taken were used to model the plates in simulation. Sample 1 has the smallest CSA and Sample 4 has the largest CSA.

Table 2 - Weld Sample Geometry

Sample No.	1	2	3	4
CSA (mm^2)	14.35	16.77	20.43	24.02
Weld Height (mm)	12.6	13	13.2	13.6
Weld Width (mm)	8.5	9.5	10.3	10.75

B. Experimental Measurement Setup

The pitch catch setup used for the 2DFFT measurements is shown in Fig. 5 and Fig. 9, where the receiver EMAT is moved

towards the weld in 1mm measurement steps. The transmitter and receiver were positioned so that the weld signal would arrive at a different time than other signals to make it easier to identify the reflected wave from edge reflections, as in experiment they cannot be prevented as they can be in simulation. Sonemat PPM EMATs, model numbers SHG2541-G and SHD2541-S with a wavelength of 25mm were used to generate Shear Horizontal modes SH0, at 128kHz, and SH1, at 205kHz. Both transmitter and receiver EMATs are constructed with two rows of six magnets, which provides narrowband excitation and reception. A LabVIEW (NI Inc., US-TX) program was used to control the wave generation parameters. The laptop used to run LabVIEW was connected to a PicoScope 5000a (PicoTech, UK) to trigger a Ritec RPR-4000 Pulser/Receiver (Ritec, INC, US-RI), shown in Fig. 9. The Ritec generates a 5-cycle sinusoidal pulse with a reception gain of 50dB. 0.5mm lift-off was created between the EMATs and the sample so that the EMATs were able to be moved easily when measuring; lift-off and movement was achieved using 0.5mm PTFE sheets. A jig setup was used to ensure collinearity between the transmitter and receiver EMAT's and to maintain 300mm centre to centre separation.

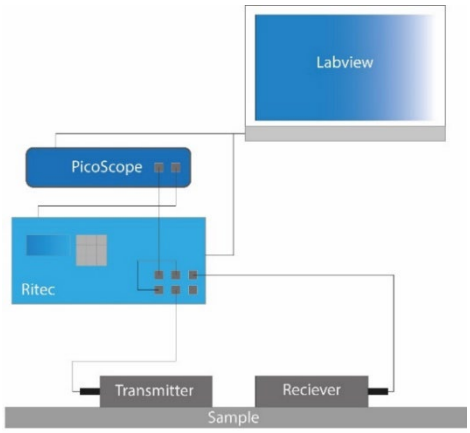

Fig. 9 Experimental setup where the LabVIEW programme is used to command the Ritec generating the pulses to send through the EMAT's. The signal from the receiver EMAT is sent to the Ritec, digitized in the Picoscope and sent back to the LabVIEW programme where it can be viewed.

C. Experimental Results and Comparison to Simulation

Experimental results are shown in Table 3. SH1 was significantly more reflective than SH0. Both modes responded to increased weld head geometry by increasing in reflectivity.

Table 3 – Experimental Reflection Coefficients

	CSA (mm^2)	SH0 (128 kHz) Experimental	SH1 (205 kHz) Experimental
Sample 1	14.35	0.145	0.409
Sample 2	16.77	0.134	0.416
Sample 3	20.43	0.188	0.442
Sample 4	24.02	0.308	0.493

As can be seen in the results there is a difference in the strength of the reflection coefficients between simulation, Fig. 8, and experiment, Table 3, there are multiple factors contributing to this increase in coefficient value.

The experimental welds are not completely consistent and have some variation in their bead size across their length, in simulation this is not the case. Real world weld variations are normal and as a result at different positions along the weld the reflection coefficient will vary slightly, this is not the case in simulation.

The plates in simulation can be considered perfect meaning there is less signal loss in the simulation sample than the physical plates, which will have many minor flaws causing additional amplitude losses.

To further validate the simulation reflection coefficients, SH0 and SH1 reflection coefficients were plotted using simulation and experimental results, shown in Fig. 10, where the results have been normalised such that the smallest reflection coefficients are given a value of 0 and the largest, a value of 1. As can be seen for both SH0 and SH1, simulation follows the same trends as experiment.

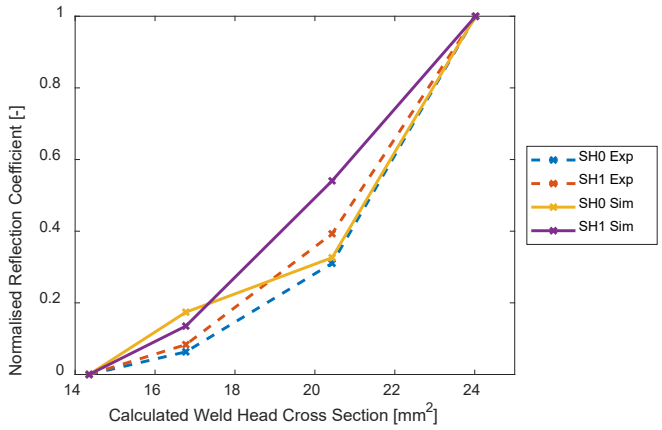

Fig. 10 Normalised reflection coefficients for SH0 and SH1 in experiment and simulation for Samples 1-4.

V. Ranging Evaluation

To evaluate the ranging capabilities of SH1, as well as SH0, waves were propagated at the weld bead from varying transmitter and receiver positions, so that relative distance between the receiver and the weld could be estimated, this is ranging. Waves of frequencies 128kHz and 205kHz were generated in Sample 4 and propagated at the weld.

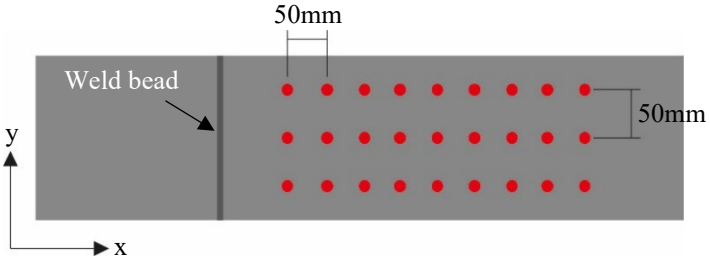

Fig. 11 Each red dot represents the positions for the receiver when propagating the modes at the weld for range and distance estimation, the transmitter and receiver EMAT's are kept 300mm apart and colinear for all measurements.

Fig. 11 shows the distinct positions of the receiver EMAT. The EMAT pair was positioned at three different points along the y-axis and moved back in 50mm steps from the weld along the x-axis, measurements further than 650mm from the weld were not carried out as the sample length did not allow it. The weld geometry is inconsistent across its length, with variation

of up to +/-2mm each side, so an average of three measurements across the weld will give a more realistic picture of a modes ranging capabilities than a signal measurement at one point.

Human error when placing the EMAT's had a contribution to the error of the modes ranging accuracy due to the high magnetic forces between the EMATs and sample. The results for the estimated and actual distances are graphed in Fig. 12.

Ranging accuracies were evaluated by comparing the actual distance and the measured distance between the weld and the receiver. A time-of-flight and Short-Time Fourier Transform (STFT) method was used to calculate the distance between the weld and the receiver using measurements [9].

A frequency time amplitude graph was formed from the measurement data using an STFT, the centre frequency of the propagated mode was then isolated across time. This forms an array of amplitude peaks which represent received waves, the peaks of the first received signal and the weld reflected signal were identified, the time between the two peaks was then calculated. Using theoretical dispersion curves the group velocity for a frequency was estimated, using the time between peaks and the group velocity the distance the wave has travelled was calculated. The difference between the calculated distance and the actual distance, which is known, can then be used to find the modes ranging accuracy.

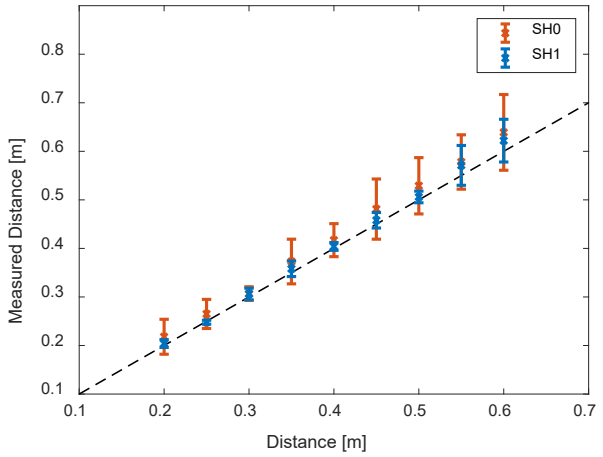

Fig. 12 Distance is the distance from receiver to the weld. Distance vs Estimated Distance of SH0, group velocity 3259m/s, orange, and SH1, group velocity 2000m/s, blue, in experiment. The dashed line shows the exact position of the weld to the centre of the EMAT.

As shown in Fig. 12, SH1 can be used to accurately estimate the distance from the receiver to the weld, better than SH0, as over the nine distances SH1 had higher positional estimation accuracy and less error throughout than SH0. The overall positional estimation error of SH1 was 2.65% and the overall positional estimation error of SH0 was 5.96%. For SH1 at an EMAT pair position ≥75cm from the weld, interpretation of the weld reflection became harder. This is thought to be due to dispersion, where the group velocity is a less accurate value to use for calculating the weld distance and the spreading out of the signals energy results in the reflection becoming a less prominent amplitude spike. It is also thought to be caused by signal attenuation, as at the point of reception the signal will have travelled >1.5m which will expectedly cause the signals amplitude to decrease.

VI. Conclusion

In order to select an optimal wave mode for the localisation of an inspection robotic platform, various guided wave modes were investigated against the weld reflection. Welds can be clearly detected using the SH1 wave mode and the position of a weld relative to the position of the receiver can be accurately estimated at the distances evaluated. SH1 is a dispersive mode, however, during experiment and simulation this was not a significant issue due to the ranges of propagation and the narrowband signal used. A 2.65% estimation error for SH1 over multiple positions is considered suitably accurate for ranging and mapping over reasonable distances that would be expected on large steel plant such as pressure vessels.

This work has drawn the following conclusions:

- SH1 is the most reflective mode, out of those tested and can be used to detect a butt-welded feature with strong certainty of the features relative position.
- A highly weld reflective mode has an energy distribution favouring the edges of the plates and has low mode conversion when encountering features.
- Compared to the SH1 wave mode, Lamb waves are not suited for use in ranging from welds. Although S1 had good reflectivity, and mode conversion occurred at this frequency making it inferior to SH0, which itself was shown to be unsuitable for ranging from welds.

Future work for this system is to develop a unique compact EMAT array with unidirectional generation where transmitter and receiver housed in the same unit. This will allow the mobile robotic system to use SH1 guided waves to identify positions of reflectors relative to itself with a simpler analysis routine, as well as compact and easy mounting.

VII. References

[1] J. M. Farley, 'BEST PRACTICE IN THE APPLICATION OF NDT – AN UPDATE', *Mitsui BabcockHSE*, p. 6, 2004.

[2] P. Horrocks, D. Mansfield, K. Parker, J. Thomson, T. Atkinson, and J. Worsley, 'Managing Ageing Plant', *HSE Books*, p. 53, Aug. 2010.

[3] F. Rubio, F. Valero, and C. Llopis-Albert, 'A review of mobile robots: Concepts, methods, theoretical framework, and applications', *Int. J. Adv. Robot. Syst.*, vol. 16, no. 2, p. 172988141983959, Mar. 2019.

[4] 'Human factors/ergonomics, health and safety in the workplace'. https://www.hse.gov.uk/humanfactors/index.htm.

[5] R. Siegwart, I. Nourbakhsh, and D. Scaramuzza, *Introduction to Autonomous Mobile Robots*, Second. The MIT Press, 2004.

[6] M. Tabatabaeipour *et al.*, 'Application of ultrasonic guided waves to robotic occupancy grid mapping', *Mech. Syst. Signal Process.*, vol. 163, p. 108151, Jan. 2022.

[7] S. Thrun, W. Burgard, and D. Fox, *Probabilistic Robotics*, 1st ed. The MIT Press, 2006.

[8] P. D. Wilcox, 'LAMB WAVE INSPECTION OF LARGE STRUCTURES USING PERMANENTLY ATTACHED TRANSDUCERS', p. 223.

[9] J. L. Rose, *Ultrasonic Guided Waves in Solid Media*. New York: Cambridge University Press, 2014. doi: 10.1017/CBO9781107273610.

[10] M. Hirao and H. Ogi, *Electromagnetic Acoustic Transducers: Noncontacting Ultrasonic Measurements using EMATs*. Tokyo: Springer Japan, 2017.

[11] H. Sun, L. Peng, J. Lin, S. Wang, W. Zhao, and S. Huang, 'Microcrack Defect Quantification Using a Focusing High-Order SH Guided Wave EMAT: The Physics-Informed Deep Neural Network GuwNet', *IEEE Trans. Ind. Inform.*, vol. 18, no. 5, pp. 3235–3247, May 2022.

[12] H. Sun, S. Huang, Q. Wang, S. Wang, and W. Zhao, 'Improvement of unidirectional focusing periodic permanent magnet shear-horizontal wave electromagnetic acoustic transducer by oblique bias magnetic field', *Sens. Actuators Phys.*, vol. 290, pp. 36–47, May 2019.

[13] K. Worden, 'Rayleigh and Lamb Waves - Basic Principles', *Strain*, vol. 37, no. 4, pp. 167–172, Nov. 2001.

[14] S. Mech, T. Michaels, J. Emmons, and M. Sugiyama, 'Development of ultrasonic examination methods for austenitic stainless steel weld inspection', HEDL-SA-1348, 5059068, Aug. 1977.

[15] D. E. Hardt and J. M. Katz, 'Ultrasonic Measurement of Weld Penetration', *Weld. Res. Suppl.*, pp. 273–280, Sep. 1984.

[16] T. J. Jessop, P. J. Mudge, and J. D. Harrison, *Ultrasonic measurement of weld flaw size*. Washington, D.C: Transportation Research Board, National Research Council, 1981.

[17] S. Halkjær, M. P. Sørensen, and W. D. Kristensen, 'The propagation of ultrasound in an austenitic weld', *Ultrasonics*, vol. 38, no. 1–8, pp. 256–261, Mar. 2000.

[18] C. R. Bird, 'Ultrasonic phased array inspection technology for the evaluation of friction stir welds', *Insight - Non-Destr. Test. Cond. Monit.*, vol. 46, no. 1, pp. 31–36, Jan. 2004.

[19] A. Erhard, G. Schenk, Th. Hauser, and U. Völz, 'New applications using phased array techniques', *Nucl. Eng. Des.*, vol. 206, no. 2–3, pp. 325–336, Jun. 2001.

[20] R. Long, J. Russell, P. Cawley, N. Habgood, D. O. Thompson, and D. E. Chimenti, 'ULTRASONIC PHASED ARRAY INSPECTION OF FLAWS ON WELD FUSION FACES USING FULL MATRIX CAPTURE', in *AIP Conference Proceedings*, Chicago (Illinois), 2009, pp. 848–855.

[21] C. M. Fortunko, 'Ultrasonic Inspection of Weldments with Frequency Scanned SH Waves', in *1979 Ultrasonics Symposium*, Sep. 1979, pp. 253–258.

[22] P. A. Petcher and S. Dixon, 'Weld defect detection using PPM EMAT generated shear horizontal ultrasound', *NDT E Int.*, vol. 74, pp. 58–65, Sep. 2015.

[23] F. Bendec, M. Peretz, and S. I. Rokhlin, 'Ultrasonic Lamb wave method sizing of spot welds', *Butterworth Co Ultrason.*, p. 7, 1984.

[24] J. P. Sargent, 'Corrosion detection in welded steel plates using Lamb waves', *Insight - Non-Destr. Test. Cond. Monit.*, vol. 52, no. 11, pp. 609–616, Nov. 2010.

[25] Y.-Q. Li, P. Zhao, Z.-Y. Qu, and G.-F. Zhai, 'Weld Defect Detection Using High Frequency SH Guided Wave Transducers Based on Magnetostrictive Mechanism', in *2017 Far East NDT New Technology & Application Forum (FENDT)*, Xi'an, Jun. 2017, pp. 26–30.

[26] D. N. Alleyne and P. Cawley, 'Optimization of lamb wave inspection techniques', *NDT E Int.*, vol. 25, no. 1, pp. 11–22, Jan. 1992.

[27] Z. Fan and M. J. S. Lowe, 'Elastic waves guided by a welded joint in a plate', *Proc. R. Soc. Math. Phys. Eng. Sci.*, vol. 465, no. 2107, pp. 2053–2068, Jul. 2009.

[28] Z. Fan and M. J. S. Lowe, 'Interaction of weld-guided waves with defects', *NDT E Int.*, vol. 47, pp. 124–133, Apr. 2012.

[29] X. Zhang and Z. Xu, 'Formation mechanism of SH guided wave in weld seam', *Results Phys.*, vol. 16, p. 102840, Mar. 2020.

[30] S.-K. Yang, P. H. Lee, J.-W. Cheng, and C.-H. Tseng, 'The Study of Wave Propagation through Plates Welded Joints Using Guided Waves SH0 Mode', *15th Asia Pac. Conf. Non-Destr. Test. APCNDT2017 Singap.*, p. 10, 2017.

[31] P. Khalili and P. Cawley, 'The choice of ultrasonic inspection method for the detection of corrosion at inaccessible locations', *NDT E Int.*, vol. 99, pp. 80–92, Oct. 2018.

[32] J. P. Sargent, 'Corrosion detection in welds and heat-affected zones using ultrasonic Lamb waves', *Insight - Non-Destr. Test. Cond. Monit.*, vol. 48, no. 3, pp. 160–167, Mar. 2006.

[33] C. Ye, Y. Zhou, V. V. B. Reddy, A. Mebane, and I. C. Ume, 'Welding induced residual stress evaluation using laser-generated Rayleigh waves', Provo, Utah, USA, 2018, p. 180003.

[34] L. J. Bond and J. Taylor, 'Interaction of Rayleigh waves with a rib attached to a plate', *Ultrasonics*, vol. 29, no. 6, pp. 451–458, Nov. 1991.

[35] 'Center for Lightweight-Production-Technology - The Dispersion Calculator: A free software for calculating dispersion curves of guided waves in multilayered composites'. https://www.dlr.de/zlp/en/desktopdefault.aspx/tabid-14332/24874_read-61142/.

[36] X. Jian, S. Dixon, N. Guo, and R. Edwards, 'Rayleigh wave interaction with surface-breaking cracks', *J. Appl. Phys.*, vol. 101, no. 6, p. 064906, Mar. 2007.

[37] I. Hajro and D. Hodzic, 'Basic Comparison of Selected Structural Steel Strength Influence On Total Welding Fabrication Costs of Oil Storage Tanks', *Trends Dev. Mach. Assoc. Technol.*, p. 4, 2008.

[38] L. Kumar, K. U. Yazar, and S. Pramanik, 'Effect of fusion and friction stir welding techniques on the microstructure, crystallographic texture and mechanical properties of mild steel', *Mater. Sci. Eng. A*, vol. 754, pp. 400–410, Apr. 2019.

[39] J. Zhang, Y. Song, X. Li, and C. Zhong, 'Comparison of Experimental Measurements of Material Grain Size Using Ultrasound', *J. Nondestruct. Eval.*, vol. 39, no. 2, p. 30, Jun. 2020.

[40] A. Huber, 'Dispersion Calculator User's Manual'. Centre for Lightweight Production Technology, Sep. 2021.

[41] Y. Cho, 'Estimation of ultrasonic guided wave mode conversion in a plate with thickness variation', *IEEE Trans. Ultrason. Ferroelectr. Freq. Control*, vol. 47, no. 3, pp. 591–603, May 2000.

[42] Y. H. Cho, W. D. Oh, and J. H. Lee, 'A Wall Thinning Detection and Quantification Based on Guided Wave Mode Conversion Features', *Key Eng. Mater.*, vol. 321–323, pp. 795–798, Oct. 2006.

[43] S. A. Uribe, N. Nakamura, H. Ogi, M. Hirao, D. O. Thompson, and D. E. Chimenti, 'MODE CONVERSION OF SH GUIDED WAVES AT DEFECTS FOR PIPELINE INSPECTION', in *AIP Conference Proceedings*, Chicago (Illinois), 2009, pp. 1550–1557.

[44] M. J. S. Lowe, D. N. Alleyne, and P. Cawley, 'The Mode Conversion of a Guided Wave by a Part-Circumferential Notch in a Pipe', *J. Appl. Mech.*, vol. 65, no. 3, pp. 649–656, Sep. 1998.

[45] P. Wilcox *et al.*, 'Guided wave testing of rail', *Insight - Non-Destr. Test. Cond. Monit.*, vol. 45, no. 6, pp. 413–420, Jun. 2003.

[46] F. Kauffmann, T. Klein, A. Klenk, and K. Maile, 'Creep behavior and in-depth microstructural characterization of dissimilar joints', *Sci. Technol. Adv. Mater.*, vol. 14, no. 1, p. 014203, Mar. 2013.

[47] C. M. Fortunko, 'Ultrasonic evaluation of austenitic stainless steel welds using shear horizontal waves', *Appl. Phys. Lett.*, vol. 39, no. 9, pp. 699–700, Nov. 1981.

[48] S. M. Tabatabaeipour and F. Honarvar, 'A comparative evaluation of ultrasonic testing of AISI 316L welds made by shielded metal arc welding and gas tungsten arc welding processes', *J. Mater. Process. Technol.*, vol. 210, no. 8, pp. 1043–1050, Jun. 2010.

[49] M. Kogia *et al.*, 'Electromagnetic Acoustic Transducers Applied to High Temperature Plates for Potential Use in the Solar Thermal Industry', *Appl. Sci.*, vol. 5, no. 4, pp. 1715–1734, Dec. 2015.

[50] Shujuan Wang, Riliang Su, Xiaoyang Chen, Lei Kang, and Guofu Zhai, 'Numerical and experimental analysis of unidirectional meander-line coil electromagnetic acoustic transducers', *IEEE Trans. Ultrason. Ferroelectr. Freq. Control*, vol. 60, no. 12, pp. 2657–2664, Dec. 2013.

[51] K. Mirkhani *et al.*, 'Optimal design of EMAT transmitters', *NDT E Int.*, vol. 37, no. 3, pp. 181–193, Apr. 2004.

[52] S. A. Ghorashi, F. Honarvar, and M. Tabatabaeipour, 'Automated extraction of local defect resonance using the principal component analysis in lock-in ultrasonic vibrothermography', *Infrared Phys. Technol.*, vol. 105, p. 103204, Mar. 2020.

[53] E. team, 'Table of material properties for structural steel S235, S275, S355, S420', *EurocodeApplied.com*. https://eurocodeapplied.com/design/en1993/steel-design-properties.

[54] P. Wilcox, M. Lowe, and P. Cawley, 'The effect of dispersion on long-range inspection using ultrasonic guided waves', *NDT E Int.*, vol. 34, no. 1, pp. 1–9, Jan. 2001.

[55] D. N. Alleyne and P. Cawley, 'A 2-dimensional Fourier transform method for the quantitative measurement of Lamb modes', in *IEEE Symposium on Ultrasonics*, Dec. 1990, pp. 1143–1146 vol.2..

[56] B. Ren, H. Cho, and C. Lissenden, 'A Guided Wave Sensor Enabling Simultaneous Wavenumber-Frequency Analysis for Both Lamb and Shear-Horizontal Waves', *Sensors*, vol. 17, no. 3, p. 488, Mar. 2017.

[57] D. Alleyne and P. Cawley, 'A two-dimensional Fourier transform method for the measurement of propagating multimode signals', *J. Acoust. Soc. Am.*, vol. 89, no. 3, pp. 1159–1168, Mar. 1991.

[58] A. Sedaghati, F. Honarvar, M. Tabatabaeipour, and A. N. Sinclair, 'Investigation of the scattering of Lamb waves from a generalized circular cavity by using Poisson/Mindlin plate theories and numerical simulation', *Proc. Inst. Mech. Eng. Part C J. Mech. Eng. Sci.*, vol. 234, no. 1, pp. 152–170, Jan. 2020.

[59] R. Halmshaw, *Non-Destructive Testing*, Second. British Institue of NDT, 2004.

VIII. Authors

Ross McMillan is currently pursuing a Doctorate with a focus on ultrasonic guided waves and EMATs for mobile robotics for non-destructive inspection. He received a M.Eng in Product Design Engineering from the University of Strathclyde in 2019.

Morteza Tabatabaeipour received his Ph.D. degree in linear and nonlinear ultrasound imaging from Katholieke Universiteit Leuven (K U Leuven) in Belgium. He is currently a Research Associate at the Centre for Ultrasonic Engineering (CUE) with the Department of Electronic and Electrical Engineering, University of Strathclyde. His primary research interests include non-destructive testing and evaluation (NDT&E), ultrasonics, thermography, structural health monitoring (SHM), robotics and automation.

Rory Hampson received the PhD and MEng degrees from the University of Strathclyde, Glasgow, U.K., in 2021 and 2017 respectively. He is currently a researcher in the Department of Electronic and Electrical Engineering at the University of Strathclyde. His current work focusses on tactile imaging for breast cancer diagnosis, medical decision making based on tactile sensor technology, and automated inspection robots. His research interests include Medical Imaging, Inertial Guidance and Control, Nuclear Inspection, and Engineering for Sustainable Development.

Charalampos Loukas is currently pursuing a Doctorate at the University of Strathclyde, focusing on robotic welding and robotic weld inspection.

Taiyi Zhao is currently pursuing a Doctorate, focusing on automated unmanned aerial vehicle deployed pulsed eddy current for non-destructive testing. He was awarded a B.Eng with first class degree in Electronic & Electrical Engineering at Strathclyde in 2019.

Rachel Edwards is Reader in Physics at the University of Warwick and obtained her PhD from the University of Oxford (UK). She moved to Warwick following a visiting researcher fellowship at the University of Florida (USA). She is a member of the Centre for Industrial Ultrasonics and the UK-based Research Centre in NDE. She has held an ERC Starting Independent Researcher Grant, and has published over 60 peer reviewed journal papers. She is very active in outreach to school students.

Charles MacLeod is a Senior Lecturer in the Centre for Ultrasonic Engineering. After being awarded a Masters in Electrical and Mechanical Engineering with Distinction at Strathclyde, Charles then went on to undertake a PhD in Automated Non-Destructive Evaluation. While undertaking his PhD Charles, was seconded to Spirit AeroSystems, in Prestwick to undertake Knowledge Exchange activities built on fundamental EPSRC funded research. Charles was awarded the prestigious University of Strathclyde EPSRC Doctoral Prize for 2014, for his work investigating automated NDE. Charles has vast experience in electrical and mechanical engineering areas such as robotics, sensors, electronics, mechanical fixturing and software.

Gordon Dobie received the Ph.D. degree in electrical and mechanical engineering from the University of Strathclyde with a focus on development of reconfigurable non-contact inspection system. He is currently a Reader with the department of Electronic and Electrical Engineering, University of Strathclyde. He is currently with CUE, where he is involved in automated ultrasonic inspection of complex geometries. His primary research interests include ultrasonics, NDE, automation, robotics, signal processing, computer vision and embedded systems.